ELSEVIER

Journal of Neuroscience Methods 157 (2006) 118–123

JOURNAL OF NEUROSCIENCE METHODS

www.elsevier.com/locate/jneumeth

Short communication

Functional cortical source imaging from simultaneously recorded ERP and fMRI

Chang-Hwan Im [a], Zhongming Liu [a], Nanyin Zhang [b], Wei Chen [b], Bin He [a,*]

[a] *Department of Biomedical Engineering, University of Minnesota, United States*
[b] *Center for Magnetic Resonance Research, University of Minnesota, United States*

Received 6 December 2005; received in revised form 5 March 2006; accepted 15 March 2006

Abstract

Feasibility of continuously and simultaneously recording visual evoked potentials (VEPs) with fMRI was assessed by quantitatively comparing cortical source images by means of receiver operating characteristic (ROC) curve analysis. The averaged EEG source images coincided well with simultaneously acquired fMRI activations. Strong correlation was found between the cortical source images of VEPs recorded inside and outside the scanner. Application of fMRI prior information strengthened correlation between estimated source images as well as resulted in source estimates with higher spatial resolution. The present results demonstrate that reliable cortical source images can be acquired during simultaneous fMRI scanning and they may be used for multimodal functional source imaging studies.

Keywords: Simultaneous fMRI and EEG; Multimodal integration; Human brain mapping; Cortical source imaging

1. Introduction

In functional neuroimaging, it is of great interest to combine multiple modalities, especially electroencephalography (EEG) and functional magnetic resonance imaging (fMRI), to take advantage of the high temporal resolution of EEG and high spatial resolution of fMRI (Babiloni et al., 2003; Bonmassar et al., 2001). For EEG–fMRI integration, it is desirable to acquire EEG and fMRI in a single session to avoid possible discrepancies due to different environmental and cognitive states in separate examinations. However, simultaneous recording of EEG and fMRI is challenging since the EEG recordings are prone to large artifacts induced by the high-frequency gradient and RF pulses inside the MR scanner, namely pulse sequence artifact (PSA), and motion of EEG leads within the static magnetic field, such as ballistocardiogram artifact (BA) caused by the pulsatile motion related to heart beat (Allen et al., 1998; Allen et al., 2000). The former artifact can be avoided using interleaved strategy such that EEG signals are recorded during the time windows in the absence of gradient and RF pulses by designing proper fMRI sequences (Bonmassar et al., 2001). Although the interleaved recording can be free from the PSA, it is often more time consuming, which is a problem in evoked potential studies that require averaging over many trials.

Efforts have been made in an attempt to design MR-compatible EEG device and develop artifact reduction post-processing techniques (Ille et al., 2002; Kim et al., 2004). Experimental studies have also been conducted using well-established paradigms that generate highly reproducible waveforms of event-related potential (ERP), such as checkerboard visual evoke potentials (VEP). Two independent studies showed that VEPs recorded inside the MR scanner (with and without simultaneous fMRI acquisition) exhibited good correlation and consistent latency and amplitude of "peaks" of waveforms at occipital electrodes (Becker et al., 2005; Comi et al., 2005). Other paradigms that elicit steady-state VEP (SSVEP), lateralized readiness potential (LRP) and frontal theta have also been adopted in another validation study, in which no substantial differences were found between the ERP signals recorded inside and outside the MRI scanning room, or with and without fMRI scanning (Sammer et al., 2005).

Since the ultimate goal of EEG–fMRI concurrent recording is to integrate these two modalities for functional neuroimaging, it is important to comparatively assess the quality of EEG signals

* Corresponding author at: Department of Biomedical Engineering, University of Minnesota, 7-105 Hasselmo Hall, 312, Church St. S.E., Minneapolis, MN 55455, USA. Tel.: +1 612 626 1115; fax: +1 612 626 6583.
E-mail address: binhe@umn.edu (B. He).

0165-0270/$ – see front matter © 2006 Elsevier B.V. All rights reserved.
doi:10.1016/j.jneumeth.2006.03.015

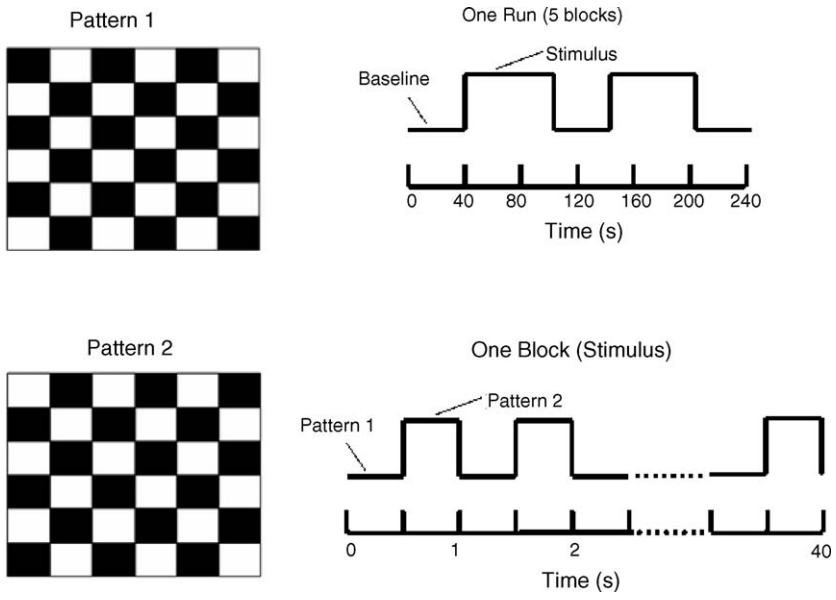

Fig. 1. Experimental design. One block composed of 2 Hz pattern reversal checkerboard stimuli (patterns 1 and 2) repeated for 40 s. Resting periods (baseline) were inserted before and after two 60 s stimulation periods lasting for 40 s, during which no visual stimuli were presented.

simultaneously recorded with fMRI in the context of EEG (or EEG–fMRI integrated) source imaging. In the present study, we explored EEG–fMRI simultaneous recording during checkerboard VEP experiments at 3T MRI scanner in human subjects. We compared the VEP waveforms acquired inside and outside MRI scanner, as well as their resulting cortical source images. The correspondence of EEG-based cortical source images and fMRI activations were also examined by means of receiver operating characteristic (ROC) curve, which shows the relationship between true and false-positive detection rates as the activation threshold of the obtained images is varied (Darvas et al., 2004; Hansen et al., 2001).

2. Materials and methods

2.1. Data acquisition

Two right-handed male human subjects (initials JS and VG; age 20 and 19 years) participated in a checkerboard visual-stimuli experiment with written consent. A full rectangular checkerboard pattern (6×6 black and white contrast, average luminance: 20 cd/m^2, flickering at 2 Hz) was delivered to the subjects through a LCD monitor outside the MRI scanning room, or back mirrored through a DLP projector inside the scanner. The horizontal and vertical visual angles of the checkerboard pattern were 40° and 30°, respectively. The subjects were instructed to fixate at a cross-mark at the center of the screen during the experiment. Three sets of EEG data were acquired (outside the MRI scanner, inside the scanner without fMRI scanning, and inside the scanner during fMRI scanning), using a 32-channel MR compatible EEG system (BrainAmp MR 32 Plus, BrainProducts, Germany). For subject VG, EEG data recorded inside the scanner without fMRI were not available. Both structure MRI (sMRI) and fMRI data were collected using a 3T MRI system (Siemens Trio, Siemens, Germany). The whole-head T1-weightd MR images (matrix size 256×256, 1 mm slice thickness) were acquired using Turboflash sequence (TR/TE = 20 ms/5 ms). The T_2^*-weighted fMRI data were acquired from 10 axial slices (matrix size 64×64, 5 mm thickness) covering visual cortex using echo planar imaging (EPI) sequence (TR/TE = 1000 ms/35 ms). We inserted resting periods before and after two 60 s stimulation periods lasting for 40 s, during which no visual stimuli were presented, to allow for a sufficient modulation of the BOLD response. Fig. 1 shows the detailed experimental design for the simultaneous EEG and fMRI acquisition. The period cross-correlation method (with the cross-correlation coefficient $\geq$0.5) was applied to obtain the fMRI activation map (Bandettini et al., 1992).

2.2. EEG signal processing

For the EEG signals continuously and simultaneously recorded with fMRI, post-processing was performed to reduce the artifacts induced by gradient and RF pulses, as well as cardiac motion. The post-processing was conducted with BrainVision Analyzer software (BrainProducts, Germany). Specifically, 25 segments of EEG signals[1] collected during the first 25 EPI volumetric acquisitions were averaged, yielding a model of PSA waveform, which was subsequently subtracted from all the recorded data during fMRI acquisition (Allen et al., 1998). The high-frequency components resulting from the above subtraction process were removed by a low-pass filter with cut-off frequency at 40 Hz. After the PSA removal process, the high frequency sampling rate (5 kHz) of the continuous signals was downsampled to 200 Hz for efficient signal processing. To correct the BA, positions of the peaks of R-wave were detected from the ECG recording (Allen et al., 2000). On each EEG channel,

[1] The length of each of the segments is the same as TR (1000 ms).

a template of the BA was built by averaging 20 epochs synchronous to the peaks of ECG R-waves (Allen et al., 1998; Allen et al., 2000). The template was then subtracted from each EEG channel considering approximately 210 ms signal delay from ECG channel to EEG channels. The continuous EEG signals were segmented with reference to the visual stimuli. Then, time segments including electrooculogram artifact (EOA) were manually rejected based upon simultaneously acquired EOG channel signal. Over 150 segments were averaged to obtain the final VEP waveforms. For the EEG signals acquired outside the scanner, only downsampling, filtering, the EOA rejection, and averaging were applied.

2.3. Cortical source imaging

The realistic-geometry (RG) three-shell head model (scalp, skull, brain) and the folded cortical surface were reconstructed from the individual subject's sMRI. A linear estimation approach (Liu et al., 2002) was used to estimate cortical current source distribution from the recorded VEP data. The source space was anatomically constrained to be on the cortical surface. The source strengths were estimated by multiplying the following linear inverse operator $\boldsymbol{W}$ with the instantaneous VEP measurements:

$$\boldsymbol{W} = \boldsymbol{R}\boldsymbol{A}^{\mathrm{T}}(\boldsymbol{A}\boldsymbol{R}\boldsymbol{A}^{\mathrm{T}} + \lambda^2\boldsymbol{C})^{-1},$$

where $\boldsymbol{A}$ is the lead field matrix which relates possible source locations to the recorded scalp potentials, $\boldsymbol{R}$ is a source covariance matrix, and $\boldsymbol{C}$ is a noise covariance matrix. $\boldsymbol{A}$ is derived from the subject-specific head model using the boundary element method (BEM) (Hämäläinen and Sarvas, 1989; He et al., 1987). The regularization parameter λ^2 was determined using the L-curve method (Hansen, 1992). Without considering fMRI priors, $\boldsymbol{R}$ is an identity matrix; when imposing fMRI constraints, the diagonal terms of $\boldsymbol{R}$ were set to 1 for source locations within fMRI activations, otherwise 0.1 (Liu et al., 2002).

3. Results and discussion

3.1. Comparison of waveforms

We first compared VEP waveforms recorded under different conditions: VEP recorded outside MRI scanner, VEP recorded inside the scanner without fMRI scanning, and VEP recorded inside the scanner during fMRI scanning. The VEP waveforms at occipital electrodes (O1, O2) for the two subjects are shown in Fig. 2a and b and Fig. 2d and e, respectively. The waveforms recorded under all three conditions were consistent with the typical VEP waveforms elicited by the checkerboard simulation. Also, their overall morphologies coincided well with each other, while slightly different latency and amplitude of P1 peak were observed (for JS, latency difference <8 ms, amplitude difference <6 μV; for VG, latency difference <2 ms, amplitude difference <5 μV). Fig. 2c and f show the fMRI activation map ($CC \geq 0.5$) projected onto the reconstructed cortical surface. For both these two subjects, the fMRI mapping

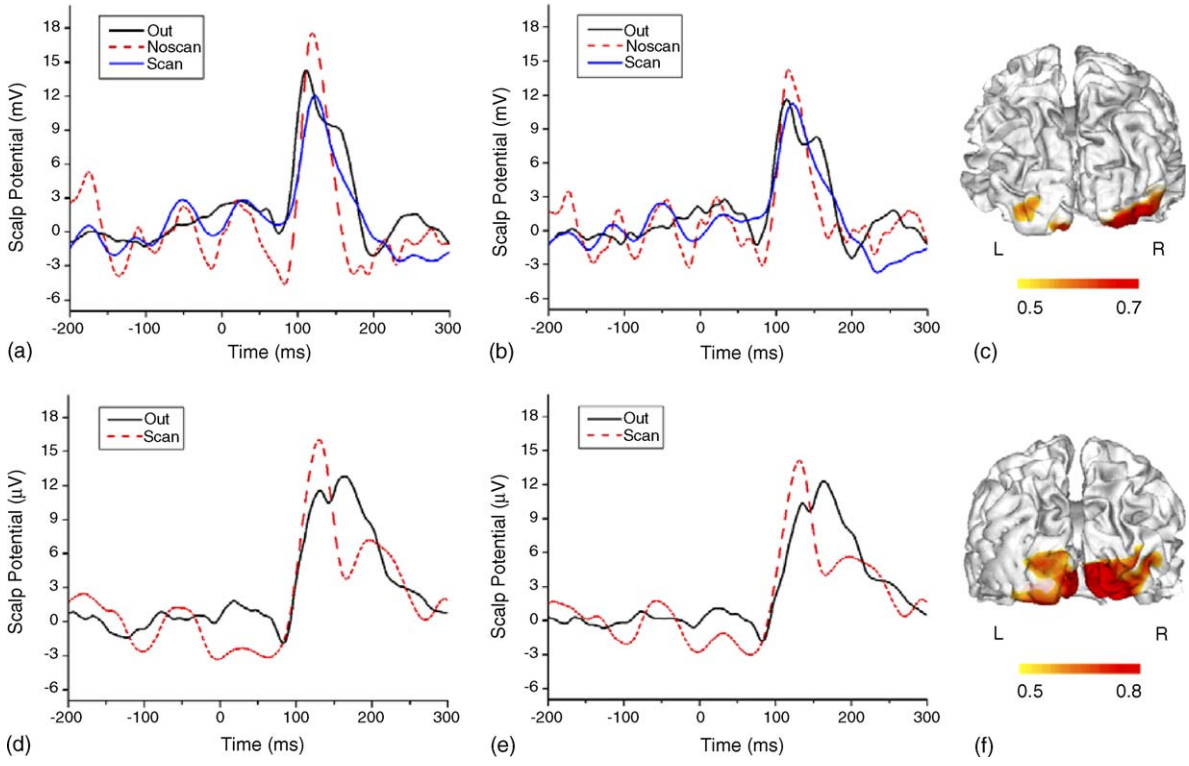

Fig. 2. VEP waveforms and fMRI maps. Subject JS: (a and b) VEP waveforms at occipital electrodes (a: O1; b: O2). (c) fMRI map projected on the subject's cortical surface. Subject VG: (d and e) VEP waveforms at occipital electrodes (d: O1; e: O2). (f) fMRI map projected on the subject's cortical surface. Out: VEP recorded outside MRI scanner; noscan: VEP recorded inside MRI scanner without scanning; scan: VEP recorded inside scanner during fMRI scanning.

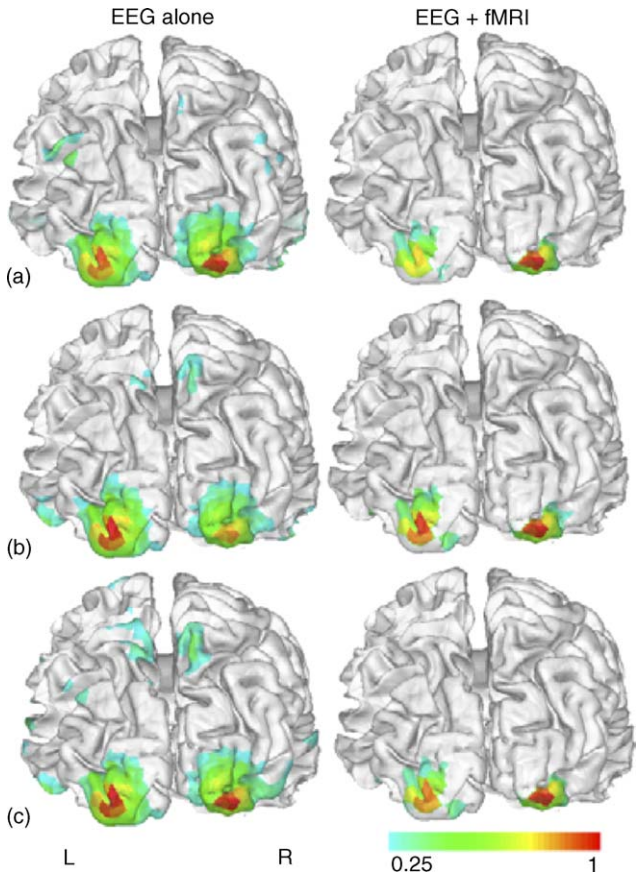

Fig. 3. Estimated cortical source images from subject JS's VEP: (a) recorded outside MRI scanner; (b) recorded inside MRI scanner without fMRI scanning; (c) recorded inside MRI scanner during fMRI scanning. The contour scales are normalized with respect to the maximum value.

shows BOLD activation at primary visual cortex, as expected, suggesting that the application of electrode cap didn't introduce significant distortions to both sMRI and fMRI.

3.2. Comparison of cortical source images

For the source estimation, relatively smaller numbers of source locations (6927 for JS; 6911 for VG) were downsampled from the fully tessellated cortical surface (694,188 triangles for JS; 623,228 triangles for VG), which was extracted using BrainSuite software package (Shattuck and Leahy, 2002). The original surface was used only for visualization purpose. We then reconstructed cortical source distributions using linear inverse estimation with and without fMRI prior constraint. The cortical source powers (square of source intensities) estimated at every time slice within [100 ms, 200 ms] were averaged, shown in Figs. 3 and 4. The averaged cortical source images were compared with fMRI activation maps to assess the correspondence between neural electrophysiological energy inversely estimated from EEG measurements and the metabolic energy consumption and hemodynamic response as indicated by BOLD-fMRI mapping (Vitacco et al., 2002). It can be clearly seen that the estimated cortical source images are similar to each other and they are corresponding well to the simultaneously

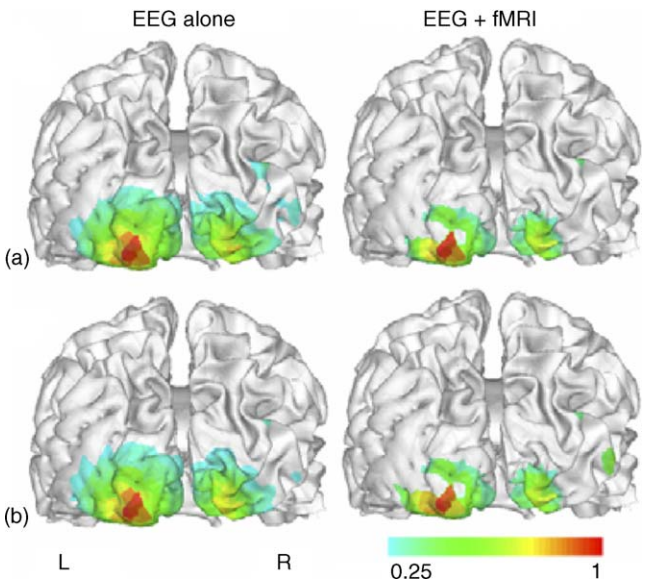

Fig. 4. Estimated cortical source images from subject VG's VEP: (a) recorded outside MRI scanner; (b) recorded inside MRI scanner during fMRI scanning. The contour scales are normalized with respect to the maximum value.

acquired fMRI map. Moreover, the extended sources became more focalized and most spurious sources were diminished by applying the fMRI constraint, as found in a previous study on the fMRI-constrained EEG source imaging (Bonmassar et al., 2001).

We then evaluated receiver operating characteristic (ROC) curves (Darvas et al., 2004; Hansen et al., 2001) between the estimated cortical source images and fMRI activation maps. The ROC curves present the relationship between false positive fraction (FPF = EEG activation outside fMRI activation/total area outside fMRI activation) and true positive fraction (TPF = common EEG and fMRI activation area/fMRI activation area). Therefore, larger area below an ROC curve means that the EEG cortical image coincides better with the fMRI activation ($0 \leq$ area below an ROC curve ≤ 1).

Fig. 5a and b show the ROC curves and areas below the curves. Clearly, the cortical source images estimated from different sets of VEP data end up with closely-correlated ROC curves, which suggests again the difference of VEP waveforms recorded with or without fMRI do not significantly affect the EEG source imaging results. In addition, the strong correspondence between fMRI activation and cortical source images obtained from EEG alone were also observed in the ROC analysis, with the area under the ROC curves being around 0.8 for JS or around 0.95 for VG. Interestingly, the fMRI-guided source estimate not only increased the correlation between EEG sources and fMRI activations but also improved the correlation between the EEG source images (smaller difference in the areas below the ROC curves). This suggests that the use of fMRI prior information diminished spurious sources, which usually stems from noisy recording environments and restricted possible source space to physiologically more probable regions.

For both two subjects, the cortical source estimates for 'inside scanner recordings' coincided better with fMRI activa-

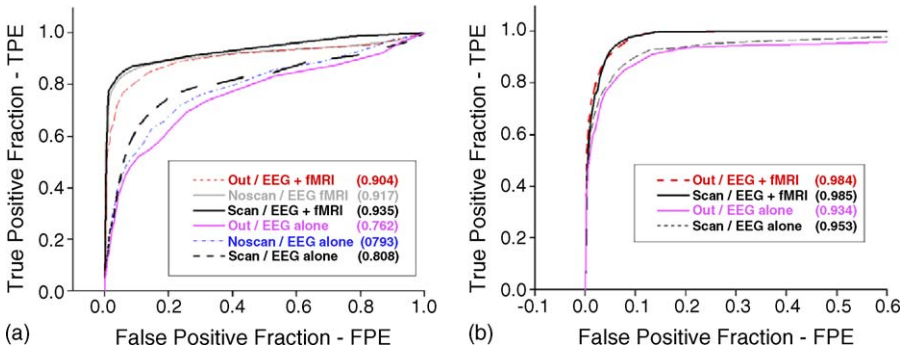

Fig. 5. ROC curves with respect to fMRI activations: (a) subject JS; (b) subject VG. The abbreviations are the same as defined in Fig. 1. Values in parentheses represent areas below ROC curves.

tion than those for 'outside recording', and the simultaneously recorded EEG and fMRI result in the best correspondence. These results further confirmed that the artifacts inherent in fMRI-EEG concurrent acquisition have been successfully removed in the present study. This inference relies on the fact that the visual evoked activities can hardly be identical from run to run as affected by unavoidable conditional differences. These include the changes of experimental environment (e.g. direct presentation on monitor versus back-mirroring) and visual stimulation (e.g. vertical and horizontal visual angles), as well as the subject's concentration. Relative to the run of fMRI scanning, these conditional differences are the largest when recording EEG outside the MRI room, the secondly largest when recording EEG alone inside the scanner, but virtually zero for simultaneous fMRI–EEG acquisition. It is hence reasonable to assume that if simultaneous recording artifacts can be effectively removed so that the conditional differences are dominant factors that claim for the discrepancy of neural activities monitored respectively by fMRI and EEG's. We can expect that the simultaneously recorded EEG should possess the best correspondence with fMRI activation, while the EEG recorded outside the MRI room exhibit the worst correspondence, as concluded in the ROC analysis of their resulting source images taking fMRI as the reference. Otherwise, if the effect of recording artifacts is dominating, the opposite finding should be expected.

4. Conclusions

In the present study, we explored the concurrent EEG–fMRI recording for two human subjects under checkerboard visual stimulation. From our comparative analysis on the VEP waveforms and their corresponding cortical source images by means of ROC curve analysis, we demonstrate that (1) VEP signals can be reliably recorded simultaneously with fMRI for the purpose of EEG-based or fMRI-EEG integrated cortical imaging; (2) the cortical source images estimated by VEP alone hold a high correspondence with fMRI activation, confirming the rationality of incorporating fMRI spatial information as constraints to EEG inverse problem; (3) the fMRI-constrained source estimate for VEP data can result in more reliable cortical images with better specificity than using VEP alone.

Acknowledgements

This work was supported in part by NSF BES-0411898, NIH RO1 EB00178, NIH RO1 EB00329, Biomedical Engineering Institute of the University of Minnesota, BTRR P41 008079, KECK Foundation and MIND Institute. CH Im was supported in part by the Korea Research Foundation Grant funded by Korea Government (MOEHRD, Basic Research Promotion Fund) (M01-2005-000-10132-0).

References

Allen PJ, Polizzi G, Krakow K, Fish DR, Lemieux L. Identification of EEG events in the MR scanner: the problem of pulse artifact and a method for its subtraction. Neuroimage 1998;8:229–39.

Allen PJ, Josephs O, Turner R. A method for removing imaging artifact from continuous EEG recorded during functional MRI. Neuroimage 2000;12:230–9.

Babiloni F, Babiloni C, Carducci F, Romani GL, Rossini PM, Angelone LM, et al. Multimodal integration of high-resolution EEG and functional magnetic resonance imaging data: a simulation study. Neuroimage 2003;19:1–15.

Bandettini PA, Wong EC, Hinks RS, Tikofsky RS, Hyde JS. Time course EPI of human brain function during task activation. Magn Reson Med 1992;25:390–7.

Becker R, Ritter P, Moosmann M, Villringer A. Visual Evoked Potentials Recovered From fMRI Scan Periods. Hum Brain Mapp 2005;26:221–30.

Bonmassar G, Schwartz DP, Liu AK, Kwong KK, Dale AM, Belliveau JW. Spatiotemporal brain imaging of visual-evoked activity using interleaved EEG and fMRI recordings. Neuroimage 2001;13:1035–43.

Comi E, Annovazzi P, Silva AM, Cursi M, Blasi V, Cadioli M, et al. Visual evoked potentials may be recorded simultaneously with fMRI scanning: a validation study. Hum Brain Mapp 2005;24:291–8.

Darvas F, Pantazis D, Kucukaltun-Yildirim E, Leahy RM. Mapping human brain function with MEG and EEG: methods and validation. Neuroimage 2004;23:S289–99.

Hämäläinen MS, Sarvas J. Realistic conductivity geometry model of the human head for interpretation of neuromagnetic data. IEEE Trans Biomed Eng 1989;36:165–71.

Hansen LK, Nielsen FA, Strother SC, Lange N. Consensus inference in neuroimaging. Neuroimage 2001;13:1212–8.

Hansen P. Analysis of discrete ill-posed problems by means of the L-curve. SIAM Rev 1992;34:561–80.

He B, Musha T, Okamoto Y, Homma S, Nakajima Y, Sato T. Electric dipole tracing in the brain by means of the boundary element method and its accuracy. IEEE Trans Biomed Eng 1987;34:406–14.

Ille N, Berg P, Scherg M. Artifact correction of the ongoing EEG using spatial filters based on artifact and brain signal topographies. J Clin Neruophysiol 2002;19:113–24.

Kim KH, Yoon HW, Park HW. Improved ballistocardiac artifact removal from the electroencephalogram recorded with fMRI. J Neurosci Methods 2004;135:193–203.

Liu AK, Dale AM, Belliveau JW. Monte Carlo simulation studies of EEG and MEG localization accuracy. Hum Brain Mapp 2002;16:47–62.

Sammer G, Blecker C, Gebhardt H, Kirsch P, Stark R, Vaitl D. Acquisition of typical EEG waveforms during fMRI: SSVEP, LRP, and frontal theta. Neuroimage 2005;24:1012–24.

Shattuck DW, Leahy RM. BrainSuite: an automated cortical surface identification tool. Med Image Anal 2002;6:129–42.

Vitacco D, Brandeis D, Pascual-Marqui R, Martin E. Correspondence of event-related potential tomography and functional magnetic resonance imaging during language processing. Hum Brain Mapp 2002;17:4–12.